

Performance comparison of new and traditional arrangements of a dish-Stirling system

Cheng Zhang^a, Ycxanping Zhang^{a,*}, Inmaculada Arauzo^b, Wei Gao^a, Chongzhe Zou^a

^aSchool of Energy and Power Engineering, Huazhong University of Science and Technology, Wuhan, China

^bCIRCE Research Institute, University of Zaragoza, Maria de Luna, Zaragoza, Spain

Abstract

The solar dish Stirling engine system is well known for its high light-to-electricity conversion efficiency. However, solar dish systems are not widely applied due to the limitation of dish collector size and Stirling engine size. This paper puts forward an effective way to overcome the limitation by using Stirling engine array (SEA) in the solar dish system to increase the power of Stirling engines. To find out the influence of connection type on the performance of SEA, five basic connection types were proposed and SEA analytical models were developed based on a proposed Stirling engine model. In the engine model, various losses and irreversibilities were analyzed. The model was evaluated by considering the prototype GPU-3 Stirling engine as a case study. Based on the SEA models, global efficiency and power of different connection types of SEAs with the same hot and cold flows were evaluated. Effects of different factors on the performance of SEA were considered. Result shows that flow order has little influence on the SEA performance, and serial flows connection type is the best for an SEA to obtain best performance and adaptability for given heating and cooling fluids.

Keywords: Stirling cycle, Stirling engine model, Stirling engine array, connection type

1. Introduction

With the emphasis on energy and environmental impact, recently gaining attention is focused on Stirling engine for its high efficiency, low maintenance requirement, ⁵ flexibility on energy sources, no pollution, low explosion risk. Due to its closed cycle, it can use almost any heat source, which makes it compatible with alternative and renewable energy sources.

The Stirling engine is widely used on solar dish system, known as dish-Stirling system. In a traditional dish-Stirling system, each Stirling engines is put on the focus of a parabolic dish to use the heat collected by the dish receiver for power generation. However, solar dish systems are not widely applied yet for its small capacity. Its capacity is mainly constrained by two factors: dish collector size and Stirling engine size. The dish size is limited for the cost and difficulty of production of large mirrors. The Stirling engine size is limited for its low power-to-weight ratio. ¹⁵ The tracking feature of dish collector limits the weight of engine on the focal point. Besides, the size of engine is limited for it overlaps part of the collector. ²⁰

This paper presents new arrangements for dish-Stirling system demonstrated in Figure 1 to solve the limitations. ²⁵ In this figure, Stirling engines are put on the ground as a Stirling engine array (SEA). Heat collected by multiple

dish collectors is supplied to the SEA by heating fluid. Since the engines are static installations on the ground where space and weight are not at a premium any more, they can reach higher capacities. They can be connected in a different connection type and their performance may be improved compared to the traditional arrangement in which they are put on the focal points of each dish collector separately.

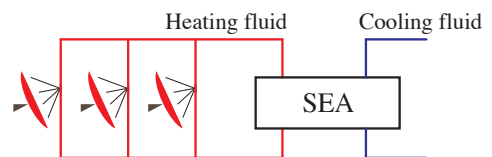


Figure 1: New arrangement of dish-Stirling system

Great attention has focused on the application using parabolic dish to collect heat. Some researchers investigated the impact of various parameters on the optical and thermal performance of the solar dish receivers using Monte Carlo Ray Tracing Method (MCRTM) and/or numerical modeling methods [1–7]. Some researchers considered the applications with different ways to use the collected heat. Loni et al. [8] considered a system using parabolic dish for an organic Rankine cycle. In the proposed system, thermal oil is used as the working fluid to transport the collected heat for the organic Rankine cycle.

*Corresponding author

Email address: zyp2817@hust.edu.cn (Ycxanping Zhang)

Wang et al. [9] proposed an inverse design method for a cavity receiver used in solar dish Brayton system. Craig et al. [10] evaluated a parabolic dish tubular receiver used₁₀₅ in a dish Brayton cycle. An approach for incorporating a complex geometry like a tubular receiver generated using CFD software into SolTrace was developed. Aichmayer et al. [11] presented a hybrid solar micro gas-turbine system integrating volumetric solar dish receiver. Concerning the₁₁₀ solar dish receiver integration, both pressurized and atmospheric configurations have been considered. Lovegrove et al. [12] presented an idea of using parabolic dish array to provide heat for ammonia based thermochemical energy storage. In this regard, using parabolic dishes to provide₁₁₅ heat for SEA is applicable.

A large number of studies have been done on Stirling engine analysis. To describe a Stirling engine's behavior precisely is a difficult task due to the various losses and irreversibilities in the engine. Researchers have done a lot₁₂₀ of work to build a precise Stirling engine model. Different models of Stirling engines were developed using empirical [13–19], analytical [20–31] and numerical methods [32–42].

Among these methods, numerical methods obtain the₁₂₅ most accurate models. Urieli and Berchowitz [32] proposed an adiabatic model of Stirling engine considering some irreversible effects such as non-ideal heat transfer processes and pressure drop effect using numerical methods. The model is known as Simple model. Many re-₁₃₀searchers developed more accurate models based on the Simple model by using alternative methods or including more loss mechanisms. Ni et al. [33] proposed an improved Simple analytical model which considers the influence mechanism of rotary speed, pressure and work-₁₃₅ing gas in the view of heat/power losses for Stirling engine performance. Jia et al. [34] developed a numerical model of free-piston engine generator. The dynamic equations have been linearized to simplify the model to a one-degree forced vibration system with various damping.₁₄₀ The solving time of the proposed fast response model can be significantly reduced comparing to previous numerical models. Strauss and Dobson [35] proposed an alternative method to calculate the regeneration heat loss and pumping losses, which is more suitable for preliminary engine₁₄₅ design and optimisation, known as Simple II model. Abbas [36] considered the effects of non-ideal regeneration, shuttle loss and heat conduction losses based on Simple model. Araoz et al. [37] developed a rigorous Stirling engine model with adiabatic working spaces, isothermal heat₁₅₀ exchangers. It considers dead volumes, and imperfect regeneration, mechanical pumping losses due to friction, limited heat transfer and thermal losses on the heat exchangers. The model is suitable for different engine configurations (α , β and γ engines). Babaelahi and Syyaadi [38] proposed a new numerical thermal model based on polytropic expansion/compression processes. Differential equations in the expansion/compression processes were modified to polytropic processes in the new model. New model shows

a better performance prediction compared with previous models.

With the development of finite-time thermodynamics, many researchers studied the finite-time thermodynamic performance of the Stirling engine. This analysis can also be used in the case of irreversible machines further considering the internal irreversibilities of a Stirling engine such as friction, pressure drop and entropy generation [39]. Wu et al. [40] developed a numerical model considering finite-time effect to find out the relationship between the net power output and thermal efficiency of the engine. Li et al. [41] developed a mathematical model of a high temperature differential dish-Stirling system with finite-time thermodynamics. Finite-rate heat transfer, regenerative heat losses, conductive thermal bridging losses and finite regeneration processes of the Stirling engine were considered in the model. Hosseinzade [42] presented a new closed-form thermal model for the thermal simulation of Stirling engines based on the combination of polytropic analysis of expansion/compression processes and the concept of finite speed thermodynamics. Instead of finite-time method, Ahmadi et al. [43] proposed a finite-speed thermodynamic analysis based on the first law of thermodynamics for a closed system with finite speed and the direct method. The effects of heat source temperature, regenerating effectiveness, volumetric ratio, piston stroke as well as rotational speed are included in the analysis. Chen et al. [44] developed a heat-engine cycle model using finite-time thermodynamics. The model, considered the losses due to heat-resistance, heat leaks and internal irreversibility, is applicable for generalized irreversible universal steady-flow heat-engine cycles.

On the other side of the researches, multi-objective optimization algorithms were used considering multi-variables to obtain a better performance was paid for attention by numbers of researchers recently [45–48]. Ahmadi et al. [45] performed the thermodynamic analysis of solar dish Stirling engine based on the finite-time thermodynamics. Then the NSGA-II algorithm was applied. Three objectives, thermal efficiency, entransy loss rate and power output, were set as the objectives and three well known decision making methods have been employed in the algorithm. Li et al. [46] developed a multi-objective optimization model of a solar energy powered gamma type Stirling engine using Finite Physical Dimensions Thermodynamics (FPDT) method by multi-objective criteria. Genetic algorithm was used to get the Pareto frontier, and optimum points were obtained using the decision different making methods. Results show that total thermal conductance, hot temperature, stroke and diameter ratios can be improved. Patel and Savsani [47] developed a strategy for multi-objective optimization for Stirling engines using TS-TLBO (tutorial training and self learning inspired teaching-learning-based optimization) algorithm. An application example with eleven decision variables and three objectives are considered. Luo et al. [48] proposed a multiple optimization method that combines multiple optimiza-

tion algorithms including differential evolution, genetic algorithm and adaptive simulated annealing. The optimization considers five decision variables, including engine frequency, mean effective pressure, temperature of heating source, number of wires in regenerator matrix, and the wire diameter of regenerator for maximum efficiency and output power.

However, the literature review indicates that the analysis of arrangements of Stirling engines, classification and performance of the SEA, has not been reported till now. In this regard, this paper investigated the connection types of SEA and its influence on SEA performance. Connection types of SEA were classified and five basic connection types were put forward. According to Organ's theory [49], one equivalent analytical Stirling engine model always exists for different types (α type, β type and γ type) of engines. To find out the influence of connection type of SEA and to avoid falling into the problem of developing specific Stirling engine model, a Stirling engine model based on some assumptions and simplifications was developed. This model was evaluated using experimental data of the General Motor GPU-3 Stirling engine prototype. Imperfect regeneration and some irreversibilities were considered. Heat transfer analysis of Stirling engine with heating and cooling fluids was also included. SEA models of different connection types were built depending on the engine model. Impacts of different parameters on the performance of these models were analyzed.

2. Connection types of SEA

For a single Stirling engine, the heat transfer processes between fluids and engine are independent and irrelevant with the direction of the flows, which means the efficiency and power are not affected by the direction of fluids. However, for an SEA, the connection type will affect the temperature profiles through the array and the specific work production, both of which will determine the efficiency and power of the SEA. It is practically significant to investigate the influence of connection type of an SEA on its performance. Using parallel flow, on the one hand, will reduce the flow rate of the fluid, which will reduce the power of each engine; however, on the other hand, will take the advantage of higher inlet heating fluid temperature (or lower inlet cooling fluid temperature), which may increase the power of each engine. friend who is Using serial flow, on the one hand, will increase the flow rate of the fluid, which will increase the power of each engine; however, on the other hand, the inlet heating fluid temperature reduces with the flow direction (or the inlet cooling fluid temperature increases with the flow direction), which leads to lower engine power along the flow direction. Using the same order will lead to largest fluid temperature difference (temperature difference of the heating and cooling fluids) at the first engines and smallest fluid temperature difference at the last engines. Using the reverse order will lead to more averaged fluid temperature differences of the

engines. For a heat exchanger, the reverse order (counter-flow), which leads to a smaller fluid temperature difference, has a better heat transfer effect for its lower exergy loss. However, for a Stirling engine, the smaller fluid temperature difference leads to lower performance due to the lower temperature difference of the working gas in the hot space and cold space. To find out the influence of connection types on the performance of SEA, it is essential to classify the connection types.

Five basic connection types of SEA were summarized according to the direction-irrelevant feature of Stirling engine, as shown in Figure 2. Type 1 is parallel flow, Type 2 is serial flows in the same order, Type 3 is serial flows in the reverse order, Type 4 is heating fluid in serial flow and cooling fluid in parallel flow and Type 5 is heating fluid in parallel flow and cooling fluid in serial flow. All other connection types are the combination of these five basic connection types. For instance, an SEA in Figure 3 is the combination of Type 2 and Type 4.

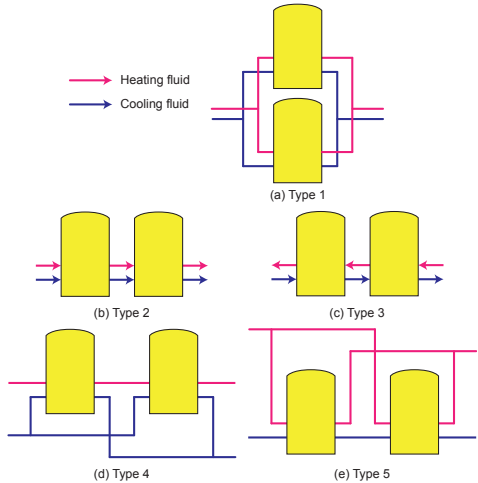


Figure 2: Five basic connection types of SEA

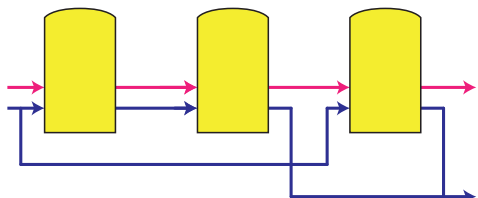


Figure 3: An instance of connection type of an SEA

3. Thermodynamic analysis of Stirling engine

3.1. Stirling engine model

3.1.1. Theoretical Stirling cycle

In a Stirling cycle, there are two isothermal processes that exchange heat with heating and cooling fluids, two isochoric processes that exchange heat with regenerator. Figure 4 shows the schematic of a Stirling cycle, process 1-2 and process 3-4 are the two isothermal processes, process 2-3 and process 4-1 are the two isochoric processes. The heat absorbed by regenerator in process 4-1 is reused in process 2-3, but only able to heat the working gas from 2 to 3' due to the imperfect regeneration. e is defined as the regenerator effectiveness for the imperfect regeneration [25], $e = \frac{T_R - T_L}{T_H - T_L}$, where T_H is the temperature in the hot space, T_L is the temperature in the cold space, T_R is the effective working fluid temperature in the regenerator.

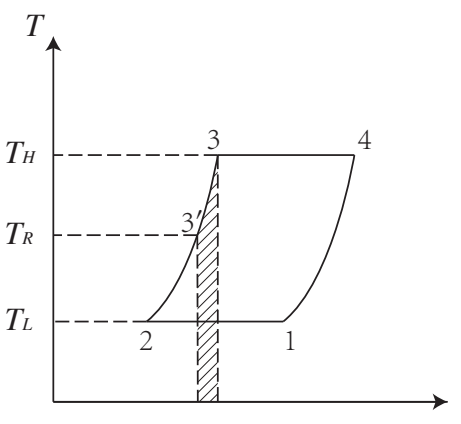


Figure 4: T - s diagram of a Stirling cycle

In order to obtain a simplified analytical model, several simplifications were made:

- The working gas in Stirling engines obeys the ideal gas law.
- No heat loss to the environment for Stirling engines.
- Overall heat transfer coefficients of the fluids are constant.
- A symmetrical regenerator behavior is assumed [25] so that a simple effectiveness can be obtain by $T_R = \frac{T_H - T_L}{\ln(T_H/T_L)}$.

To consider internal irreversibilities in Stirling cycle made by dead volumes, as described in [50], total dead volume V_D is divided into heater dead volume V_{DH} , regenerator dead volume V_{DR} and cooler dead volume V_{DC} . There exists a factor K to describe the dead volumes under

different temperatures. K is relevant with temperatures in the process and regenerator effectiveness.

$$K = \frac{V_{DH}}{T_H} + \frac{V_{DR}}{T_R} + \frac{V_{DC}}{T_L} \quad (1)$$

For the isothermal compression process 1-2, the output work

$$W_{12} = \int_{V_E+V_C}^{V_E} p_{12} dV = -mRT_L \ln \frac{V_E + V_C + KT_L}{V_E + KT_L} \quad (2)$$

For the isothermal expansion process 3-4, the output work

$$W_{34} = \int_{V_E}^{V_E+V_C} p_{34} dV = mRT_H \ln \frac{V_E + V_C + KT_H}{V_E + KT_H} \quad (3)$$

Define $\gamma_H = \frac{V_E + V_C + KT_H}{V_E + KT_H}$, and $\gamma_L = \frac{V_E + V_C + KT_L}{V_E + KT_L}$, so in a cycle, the theoretical output work

$$W_{th} = W_{12} + W_{34} = mR(T_H \ln \gamma_H - T_L \ln \gamma_L) \quad (4)$$

For the isochoric heating process 3'-3, the absorbed heat

$$Q_{3'3} = nc_v(T_H - T_R) = \frac{1-e}{k-1}mR(T_H - T_L) \quad (5)$$

For the isothermal expansion process 3-4, the absorbed heat

$$Q_{34} = W_{34} = mRT_H \ln \gamma_H \quad (6)$$

In a cycle, the theoretical absorbed heat

$$Q_{th} = Q_{3'3} + Q_{34} = \frac{1-e}{k-1}mR(T_H - T_L) + mRT_H \ln \gamma_H \quad (7)$$

3.1.2. Irreversibilities and losses

a. Non-ideal heat transfer effect

Because of non-ideal heater and cooler, the working fluid temperature (T_H/T_L) in these two heat exchangers is less/higher than the wall temperature (T_{hw}/T_{cw}), respectively. And T_H and T_L can be corrected by the wall temperatures as follows:

$$T_H = T_{hw} - \frac{Qs_{se}}{h_h A_{hw}} \quad (8)$$

$$T_L = T_{cw} + \frac{(Q - W)s_{se}}{h_c A_{cw}} \quad (9)$$

295 The heat transfer coefficient can be obtained using the
following correlation [38]:

$$h_{h,c} = \frac{\mu c_p f_{Re}}{2D_{h,c} Pr_{h,c}} \quad (10)$$

where f_{Re} is a Reynolds friction factor defined as:

$$f_{Re} = 0.0791 Re_{h,c}^{0.75} \quad (11)$$

300 $Re_{h,c}$, $Pr_{h,c}$ and $D_{h,c}$ are Reynolds number, Prandtl
number and hydraulic diameter of the heater/cooler ex-
changer.

b. Effect of pressure drop

305 Pressure drops in the heat exchangers cause power losses
of the Stirling engine. The pressure drops can be ob-
tained by [32]:

$$\Delta p = -\frac{2f_{Re}\mu uV}{d^2 A} \quad (12)$$

345 where u is the working gas speed, V is volume, A is
flow cross-section area.

310 The net power loss of the Stirling engine due to pressure
drop of the heat exchangers can be evaluated by:

$$W_{pd} = \oint \sum_{i=E,C} (\Delta p_i \frac{dV_i}{d\theta}) d\theta \quad (13)$$

c. Effect of finite speed of piston and mechanical friction

350 Due to the finite speed of piston, the pressure on the
piston surface is different from the pressure of ex-
pansion and compression spaces. It has been demonstrated
that the pressure on the piston surface in the expansion
process is less than the mean pressure in the expansion
space. Similarly, the pressure on the piston surface in
the compression process is greater than the mean pres-
sure in the compression space. This means the output
work is less than the theoretical value. Besides, The
output work also reduces due to mechanical friction.
The output work loss due to finite speed of piston and
mechanical friction can be obtained as follows [38]:

$$W_{fs} = \oint p(\pm \frac{au_p}{c} \pm \frac{\Delta p_f}{p}) dV \quad (14)$$

325 where the sign (+) is used in the compression space,
and the sign (-) is used in the expansion space. p is
the mean pressure in the compression/expansion space,
 u_p is velocity of the piston, c is the average speed of
molecules and Δp_f is the pressure loss due to me-
chanical friction. Δp_f , a and c can be obtained by [51]:

$$\Delta p_f = 0.97 + 0.009 s_{se} \quad (15)$$

$$a = \sqrt{3k} \quad (16)$$

$$c = \sqrt{3RT} \quad (17)$$

330 d. Energy losses due to internal conduction

The temperature differs from the heater and cooler,
heat losses from heater to cooler exists due to inter-
nal conduction through the walls of regenerator. [35]
The internal conduction loss in a cycle can be obtained
by follows:

$$Q_{id} = \frac{k_r A_r}{L_r s_{se}} (T_{hw} - T_{cw}) \quad (18)$$

where, k_r , A_r and L_r denote the regenerator matrix
conductivity, regenerator length, and regenerator con-
ductive area respectively.

e. Energy losses due to shuttle conduction

The displacer shuttles between the expansion and com-
pression space. It absorbs heat during the hot end of its
stroke and releases it during the cold end of its stroke.
This heat loss can be estimated as [52]:

$$Q_{sc} = 0.4 \frac{Z^2 k_p D_p}{J L_d s_{se}} (T_H - T_L) \quad (19)$$

where, Z , k_p , D_p , J and L_d denote the displacer stroke,
piston thermal conductivity, displacer diameter, gap
between the displacer and the cylinder, and length of
the displacer respectively.

So, in a Stirling engine, the total absorbed heat in a
cycle

$$Q = Q_{th} + Q_{id} + Q_{sc} \quad (20)$$

the output work

$$W = W_{th} - W_{pd} - W_{fs} \quad (21)$$

Power of the Stirling engine

$$P = W s_{se} \quad (22)$$

Efficiency of the Stirling engine

$$\eta = W/Q \quad (23)$$

3.2. Model validation

Evaluation of the developed thermal model was per-
formed by considering the GPU-3 Stirling engine as a case
study. Design specifications of the GPU-3 Stirling engine
are indicated in Table 1. The thermal efficiency and power
of the proposed Stirling engine model was compared with
previous thermal models and experimental data as shown
in Table 2 and Table 3.

It can be found that the proposed model has much bet-
ter agreement with the experimental results than previous
thermal models at various rotation speeds and mean effec-
tive pressures. It is required to mention that in all thermal
models both power W and input heat Q were determined
by the thermal process of heat transfer between the wall
and working gas. In the proposed model, W and Q are

Table 1: Design specifications of the GPU-3 Stirling engine [38, 53]

| Parameter | Value |
|--|-----------------------------------|
| Engine type | β |
| Working gas | Helium |
| Mass of the working gas | 1.136 g |
| <i>Heater</i> | |
| Number of tubes | 40 |
| Tube external diameter | 4.83×10^{-3} m |
| Tube internal diameter | 3.02×10^{-3} m |
| Tube length (cylinder side) | 0.1164 m |
| Tube length (regenerator side) | 0.1289 m |
| <i>Cooler</i> | |
| Number of tubes | 312 |
| Tube external diameter | 1.59×10^{-3} m |
| Tube internal diameter | 1.09×10^{-3} m |
| Average tube length | 4.61×10^{-2} m |
| <i>Regenerator</i> | |
| Number of regenerator | 8 |
| Regenerator internal diameter | 2.26×10^{-2} m |
| Regenerator length | 2.26×10^{-2} m |
| Diameter of regenerator tube | 4×10^{-5} m |
| Material | Stainless steel |
| <i>Volume</i> | |
| Swept Vol. (expansion/compression) | 120.82/114.13 cm ³ |
| Clearance Vol. (expansion/compression) | 30.52/28.68 cm ³ |
| Dead Vol. (heater/cooler/regenerator) | 70.28/13.18/50.55 cm ³ |

 Table 2: Thermal efficiency of the proposed Stirling engine model, previous thermal models and experimental data(at $T_{hw} = 922$ K and $T_{cw} = 288$ K)

| Rotation speed (Hz) | Mean effective pressure (MPa) | Thermal efficiency predicted by the simple analysis (variable Pr [32]) | | | Thermal efficiency predicted by the adiabatic analysis (simple II [35]) | | | Thermal efficiency predicted by the proposed Stirling Engine model | | | Experimental efficiency [38] |
|---------------------|-------------------------------|--|-----------|-------------------|---|-----------|-------------------|--|-----------|-------------------|------------------------------|
| | | Value (%) | Error (%) | Average error (%) | Value (%) | Error (%) | Average error (%) | Value (%) | Error (%) | Average error (%) | |
| 16.67 | 2.76 | 38.72 | 18.22 | | 32.48 | 11.98 | | 28.16 | 7.66 | | 20.50 |
| 25.00 | | 36.16 | 15.46 | | 31.21 | 10.51 | | 27.75 | 7.05 | | 20.70 |
| 33.33 | | 33.79 | 15.79 | 17.90 | 29.45 | 11.45 | 12.85 | 27.43 | 9.43 | 12.10 | 18.00 |
| 41.67 | | 31.48 | 16.28 | | 27.45 | 12.25 | | 27.17 | 11.97 | | 15.20 |
| 50.00 | | 29.12 | 17.32 | | 25.21 | 13.41 | | 26.94 | 15.14 | | 11.80 |
| 58.33 | | 29.74 | 24.34 | | 22.89 | 17.49 | | 26.74 | 21.34 | | 5.40 |
| 25.00 | 4.14 | 35.65 | 10.85 | | 32.29 | 7.49 | | 27.29 | 2.49 | | 24.80 |
| 33.33 | | 33.52 | 9.62 | | 30.40 | 6.50 | | 26.94 | 3.04 | | 23.90 |
| 41.67 | | 31.48 | 10.18 | 11.46 | 28.39 | 7.09 | 8.28 | 26.65 | 5.35 | 6.65 | 21.30 |
| 50.00 | | 29.45 | 11.25 | | 26.33 | 8.13 | | 26.39 | 8.19 | | 18.20 |
| 58.33 | | 27.40 | 15.40 | | 24.21 | 12.21 | | 26.17 | 14.17 | | 12.00 |
| 41.67 | 5.52 | 31.20 | 8.70 | | 28.59 | 6.09 | | 26.24 | 3.74 | | 22.50 |
| 50.00 | | 29.33 | 10.53 | 10.82 | 26.62 | 7.82 | 8.11 | 25.97 | 7.17 | 7.48 | 18.80 |
| 58.33 | | 27.44 | 13.24 | | 24.62 | 10.42 | | 25.73 | 11.53 | | 14.20 |
| 50.00 | 6.90 | 29.07 | 10.37 | 11.73 | 26.61 | 7.91 | 9.19 | 25.62 | 6.92 | 9.05 | 18.70 |
| 58.33 | | 27.29 | 13.09 | | 24.67 | 10.47 | | 25.37 | 11.17 | | 14.20 |

Table 3: Output power of the proposed Stirling engine model, previous thermal models and experimental data(at $T_{hw} = 922\text{ K}$ and $T_{cw} = 288\text{ K}$)

| Rotation speed (Hz) | Mean effective pressure (MPa) | Output power predicted by the simple analysis (variable Pr [32]) | | | Output power predicted by the adiabatic analysis (simple II [35]) | | | Output power predicted by the proposed Stirling Engine model | | | Experimental output power (kW) [38] |
|---------------------|-------------------------------|--|-----------|-------------------|---|-----------|-------------------|--|-----------|-------------------|-------------------------------------|
| | | Value (kW) | Error (%) | Average error (%) | Value (kW) | Error (%) | Average error (%) | Value (kW) | Error (%) | Average error (%) | Actual value (kW) |
| 16.67 | 2.76 | 1.796 | 119.02 | | 1.772 | 116.10 | | 0.861 | 4.98 | | 0.82 |
| 25.00 | | 2.555 | 128.13 | | 2.500 | 123.21 | | 1.253 | 11.88 | | 1.12 |
| 33.33 | | 3.215 | 165.70 | 272.03 | 3.117 | 157.60 | 254.71 | 1.632 | 34.88 | 104.84 | 1.21 |
| 41.67 | | 3.769 | 211.49 | | 3.615 | 198.76 | | 2.001 | 65.37 | | 1.21 |
| 50.00 | | 4.195 | 303.37 | | 3.973 | 282.08 | | 2.362 | 127.12 | | 1.04 |
| 58.33 | | 4.505 | 704.46 | | 4.203 | 650.54 | | 2.715 | 384.82 | | 0.56 |
| 25.00 | 4.14 | 3.844 | 114.75 | | 3.761 | 110.11 | | 1.818 | 1.56 | | 1.79 |
| 33.33 | | 4.856 | 120.73 | | 4.708 | 114.00 | | 2.362 | 7.36 | | 2.20 |
| 41.67 | | 5.734 | 136.94 | 259.70 | 5.501 | 127.31 | 158.41 | 2.890 | 19.42 | 39.83 | 2.42 |
| 50.00 | | 6.462 | 174.98 | | 6.126 | 160.68 | | 3.405 | 44.89 | | 2.35 |
| 58.33 | | 7.030 | 306.36 | | 6.573 | 279.94 | | 3.908 | 125.90 | | 1.73 |
| 41.67 | 5.52 | 7.645 | 133.08 | | 7.334 | 123.60 | | 3.742 | 14.09 | | 3.28 |
| 50.00 | | 8.655 | 163.87 | 180.02 | 8.206 | 150.18 | 164.91 | 4.401 | 34.18 | 43.68 | 3.28 |
| 58.33 | | 9.470 | 243.12 | | 8.858 | 220.94 | | 5.045 | 82.79 | | 2.76 |
| 50.00 | 6.90 | 10.788 | 174.50 | 287.04 | 10.223 | 160.13 | 263.63 | 5.362 | 36.44 | 97.75 | 3.93 |
| 58.33 | | 11.840 | 399.58 | | 11.071 | 367.13 | | 6.140 | 159.07 | | 2.37 |

obtained by Equation 8 and 9. Therefore all the three parameters W , Q and η are determined by the thermal model and input parameters to the model. These input parameters includes heater, cooler, mean effective pressure, type of working gas and geometrical specification of the engine.

Table 2 and 3 indicate that when mean effective pressure of the engine increases from 2.76 MPa to 6.90 MPa, best performance (efficiency and power) prediction of the proposed model exists. When rotation speed increases from 16.67 Hz to 58.33 Hz, error in prediction of performance of the proposed model increases. The proposed model may have the best performance prediction at a low rotation speed, with mean effective pressure between 4.14 MPa and 5.52 MPa.

However, there is still some discrepancy between the simulation results of proposed model and the experimental data. In the future researches, more accurate models of Stirling engine may be developed by considering other irreversibilities such as heat loss to the environment, gas spring hysteresis, and etc. It is worth pointing that there are more accurate Stirling engine models. For example, polytropic simulation models of Stirling engine show higher accuracy than our proposed model [38, 42]. However, the model needs more costly calculations and the polytropic indexes are engine-specific.

3.3. Heat transfer between the engine and the fluids

For a Stirling engine thermal process, the wall temperatures of the heater and cooler are considered to be uniform and constant. The heat transferred between the wall and the fluids is

$$(T_w - T)UdA = q_m c_p dT \quad (24)$$

with $T(0) = T_i$, $T(A) = T_o$,

$$\frac{T_o - T_w}{T_i - T_w} = \exp\left(-\frac{UA}{q_m c_p}\right) \quad (25)$$

For a Stirling engine, T_{hw} or T_{cw} can be used to substitute T_w to get the relationships between $T_{i,h}$, $T_{o,h}$ and T_{hw} , or $T_{i,c}$, $T_{o,c}$ and T_{cw} respectively.

$$\frac{T_{o,h} - T_{hw}}{T_{i,h} - T_{hw}} = \exp\left(-\frac{U_h A_h}{q_{m,h} c_{p,h}}\right) \quad (26)$$

$$\frac{T_{o,c} - T_{cw}}{T_{i,c} - T_{cw}} = \exp\left(-\frac{U_c A_c}{q_{m,c} c_{p,c}}\right) \quad (27)$$

Heat transferred from heating fluid to Stirling engine in a cycle

$$q_{m,h} c_{p,h} (T_{i,h} - T_{o,h}) / s_{se} = Q \quad (28)$$

Heat transferred from Stirling engine to cooling fluid in a cycle

$$q_{m,c} c_{p,c} (T_{o,c} - T_{i,c}) / s_{se} = Q - W \quad (29)$$

4. Modeling of the SEAs

As mentioned in section 2, there are five basic connection types for an SEA. All other connection types are

410 the combination of these five basic connection types. This paper investigates the five basic connection types.

To determine the performance of an SEA, models of all the Stirling engines need to be built depending on their thermodynamic characteristic. Stirling engines are chosen to have the same parameters including the same speed s_{se} . This is a reasonable assumption when using SEA for power generation, where the output power frequency should be constant. The speed of Stirling engine can be calibrated by speed controller system [54]. To eliminate interference of other factors, heating and cooling fluids are chosen to have same parameters for different connection types of SEAs. To clearly find out the performance differences of different SEAs, large temperature differences of the heating/cooling fluids after heat exchange with the engines are preferred. Air was chosen as the cooling fluid instead of commonly used water to avoid small temperature rise and evaporation in the cooling process. Design parameters of Stirling engines are the same as shown in Table 1. Other parameters of Stirling engines and heating/cooling fluids in SEAs are shown in Table 4. Rotation speed of the engines and mean effective pressure were chosen to be 25 Hz and 5 MPa respectively to get the best Stirling engine model for performance prediction, as pointed in section 3.2.

Table 4: Parameters of SEA models

| Parameter | Value | Parameter | Value |
|---------------|---------|-----------|--------------------|
| Heating fluid | Air | $q_{m,h}$ | 0.4 kg/s |
| Cooling fluid | Air | $T_{i,h}$ | 1000 K |
| n_{se} | 6 | $p_{i,h}$ | 5×10^5 Pa |
| s_{se} | 25 Hz | $q_{m,c}$ | 0.4 kg/s |
| p_{se} | 5 MPa | $T_{i,c}$ | 300 K |
| $U_h A_h$ | 180 W/K | $p_{i,c}$ | 5×10^5 Pa |
| $U_c A_c$ | 180 W/K | | |

In an SEA, there are 2 flows as shown in Figure 2.

435 In a serial flow, each engine's mass flow rate is q_m , and from the flow's direction, for $2 \leq x \leq n_{se}$, $T_{i,x} = T_{o,x-1}$. In a parallel flow, each engine's mass flow is q_m/n_{se} , for $2 \leq x \leq n_{se}$, $T_{i,x} = T_{i,h}$.

MATLAB was used as the programming tool to build

440 the model of SEAs, and CoolProp was used to provide fluid properties for MATLAB program. Five basic SEA models composed of the aforementioned Stirling engines and fluids were built. To compare SEA connection types under various conditions, several parameters are investigated to find out their effects on SEA performance.

Figure 5 shows the solution algorithm of the SEA model. Flowchart (a) shows the algorithm to solve a Stirling engine known inlet parameters of the fluids. Flowchart (b) shows the algorithm to solve a Stirling engine known in-
450 let parameters of heating fluid and outlet parameters of cooling fluid. Flowchart (c) shows the algorithm to solve

the SEA model iteratively depending on different connection types. The levenberg-marquardt algorithm is applied to numerically solve the non-linear equations in the flowcharts.

5. Result Analysis

SEA models with specified parameters in Table 4 were built and calculated. Results of the performances of the SEAs are shown in Table 5, it can be found that under specified parameters Type 3 has the highest efficiency and output power, while Type 1 has the lowest efficiency and output power.

Table 5: Results of SEA models under specified parameters

| Parameter | Value | Parameter | Value |
|-----------|--------|-----------|--------|
| η_1 | 0.2215 | P_1 | 8022 W |
| η_2 | 0.2273 | P_2 | 8483 W |
| η_3 | 0.2277 | P_3 | 8512 W |
| η_4 | 0.2227 | P_4 | 8116 W |
| η_5 | 0.2263 | P_5 | 8399 W |

5.1. Effects of $T_{i,h}$

According to Carnot cycle efficiency formula, the temperature of heating fluid determines the efficiency of Stirling engine array. For a Stirling engine, lower temperature heating fluid leads to a lower efficiency. The efficiency and output power may drop to 0 due to its insufficient heating fluid temperature to drive the engine.

Curves of performance of SEAs and $T_{i,h}$ are shown in Figure 6. As it is shown, with the increase of $T_{i,h}$, both η and P increase for all SEAs. For some types of SEA, when $T_{i,h}$ is lower than a critical temperature, some of the engines in the SEA will not work and there will be turning points on the $\eta - T_{i,h}$, $P - T_{i,h}$ curves. E.g. for SEA of Type 1, when $T_{i,h}$ is lower 820 K, all the engines stop working, turning points at 820 K can be found on the $\eta - T_{i,h}$, $P - T_{i,h}$ curves in Figure 6.

From curves in Figure 6, it can be concluded that Type 2 and Type 3 have the best performance, and Type 2 has the best adaptability for lower $T_{i,h}$. All engines in Type 2 begin to work at 730 K.

5.2. Effects of $q_m c_p$

According to Equation 28, 29, $q_m c_p$ (both $q_{m,h} c_{p,h}$ and $q_{m,c} c_{p,c}$) will affect the heat transfer process, which is one of the vital factor for the performance of SEA.

Curves of performance of SEAs and $q_{m,h} c_{p,h}$ are shown in Figure 7. For a large $q_{m,h} c_{p,h}$ (> 800 W/K), Type 2, Type 3 and Type 5 have similar performance, which can be

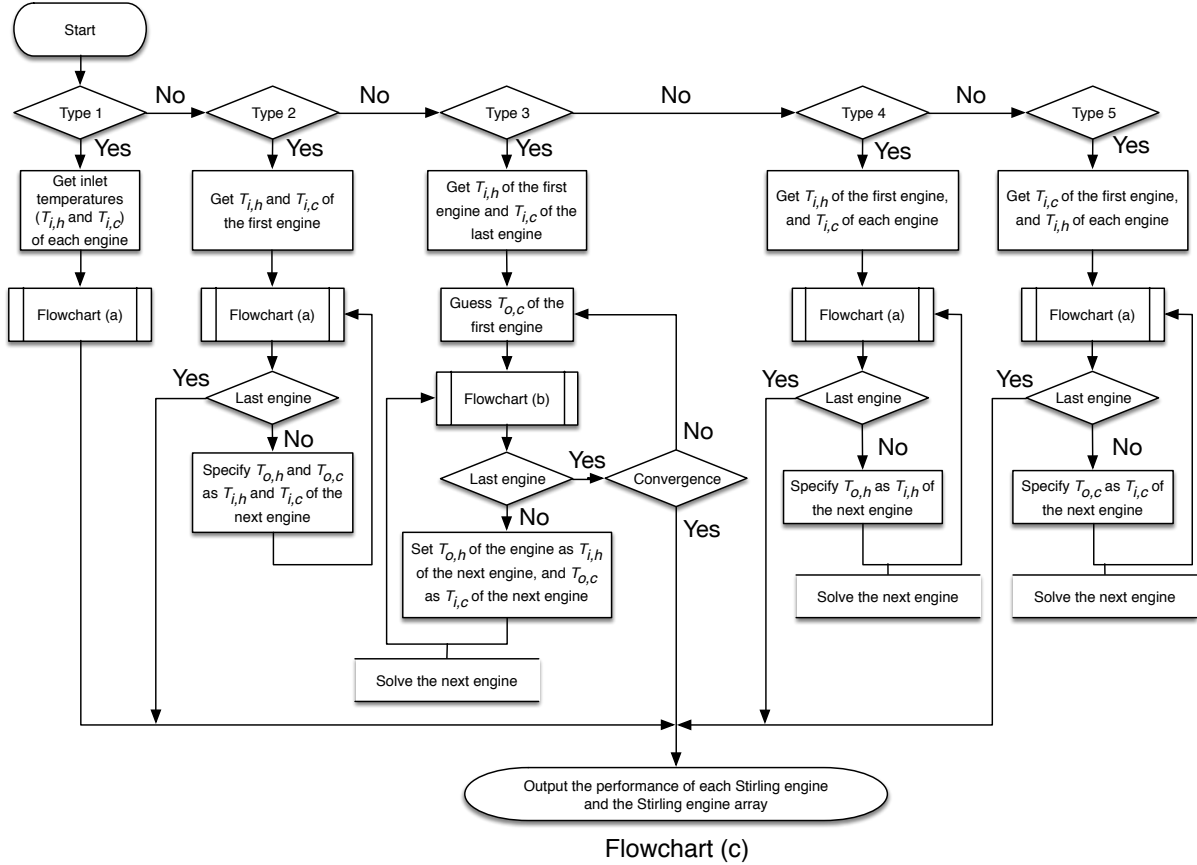
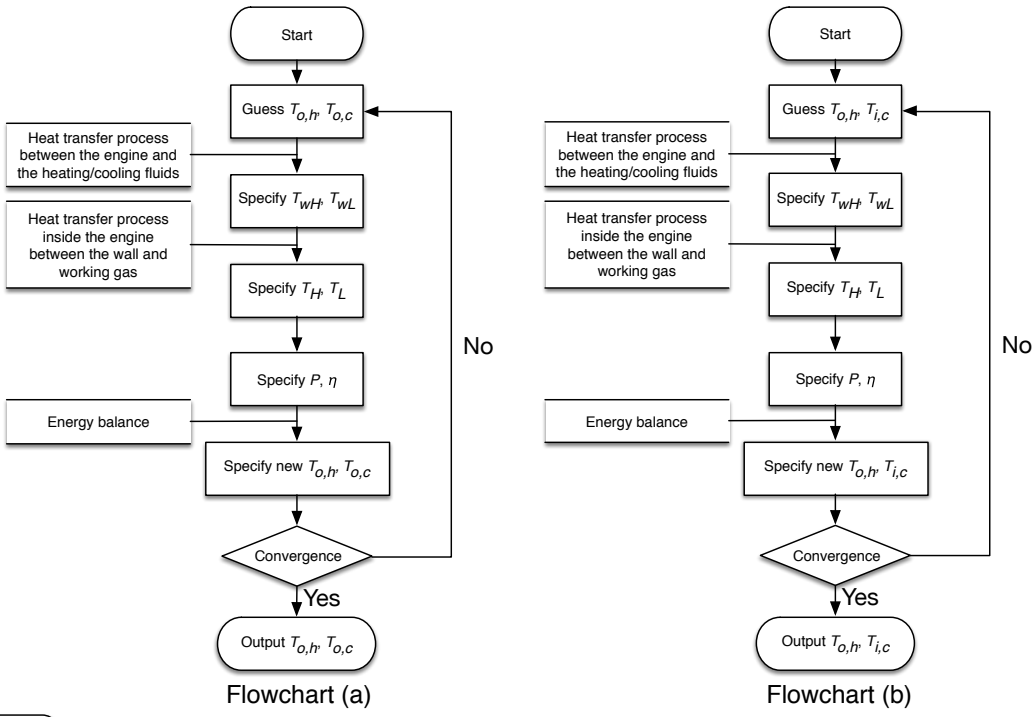


Figure 5: Flowcharts of the SEA model for performance analysis of the SEAs

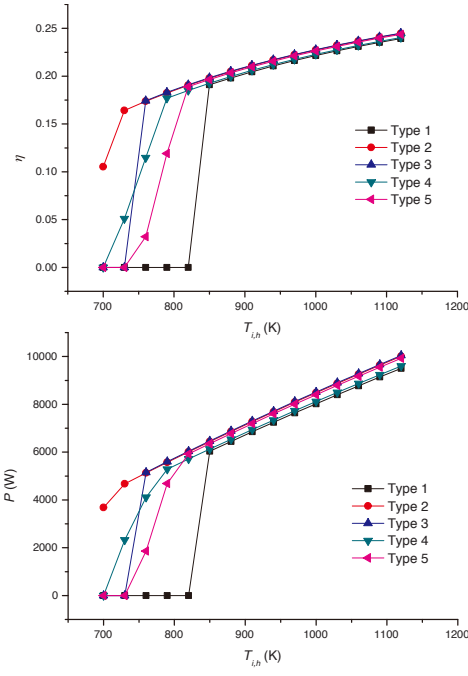


Figure 6: Influence of $T_{i,h}$ on efficiency and power of SEA

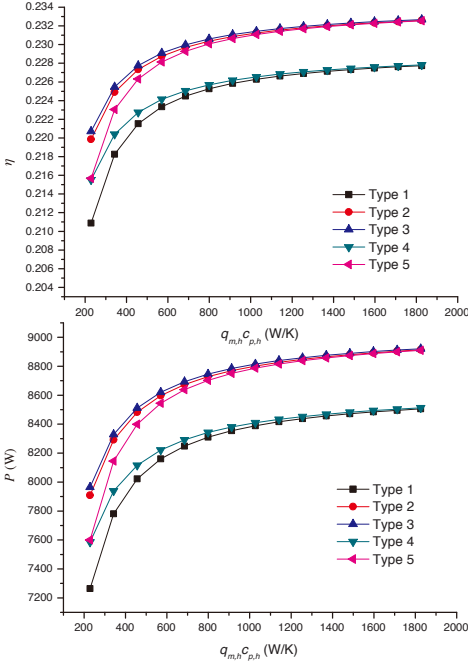


Figure 7: Influence of $q_{m,h}c_{p,h}$ on efficiency and power of SEA

interpreted as the cooling fluid has the same properties for the two types of SEAs, and for a large $q_{m,h}c_{p,h}$, the heating fluid has similar effect after diverged. Similar performance of Type 1 and Type 4 can be also interpreted for the same reason.

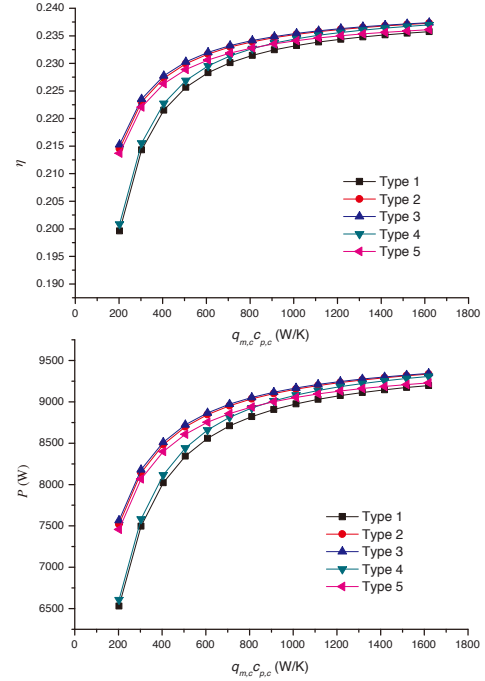


Figure 8: Influence of $q_{m,c}c_{p,c}$ on efficiency and power of SEA

Curves of performance of SEAs and $q_{m,c}c_{p,c}$ are shown in Figure 8. For a connection type of SEA, the performance improves with the increase of $q_{m,c}c_{p,c}$. For a large $q_{m,c}c_{p,c}$ (> 800 W/K), Type 2 and Type 3 have similar performance, which means the flow order doesn't affect the performance of SEA with a large $q_{m,c}c_{p,c}$. There exists an intersection point (at 830 W/K) of curves of Type 4 and Type 5. For a larger $q_{m,c}c_{p,c}$, Type 4 has a better performance, and vice versa. This can be interpreted that larger $q_{m,c}c_{p,c}$ weaken the drawback of larger temperature rise of parallel flow, while for the heating fluid, temperature drop of serial flow is smaller than parallel flow.

5.3. Effects of n_{se}

By varying the number of engines in SEA, the performance levels changed accordingly. n_{se} may affect both the flow rates and temperatures of fluids of each engine. Figure 9 shows curves of performance of SEAs with different n_{se} . As it is shown, with an increase of n_{se} leads to a reduction of η for all SEAs due to smaller heating and cooling average temperature difference for more engines. For some types of SEA, when n_{se} is larger than a critical value, some of the engines in the SEA will not work and the curves will dive. E.g. for SEA of Type 1, when n_{se} is

larger than 9, all the engines stop working, turning points at 9 can be found on the $\eta - n_{se}$, $P - n_{se}$ curves in Figure 9.

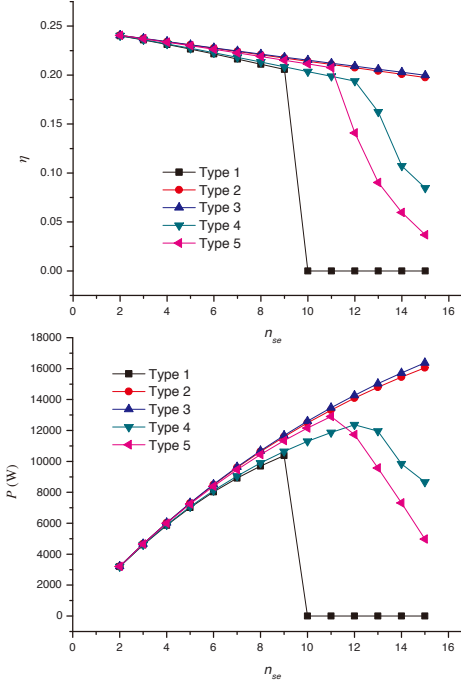


Figure 9: Influence of n_{se} on efficiency and power of SEA

For Type 1, when $n_{se} \geq 10$, all engines stop working. For given heating and cooling fluids due to small $q_m c_p$. For Type 2 and Type 3, every engine in the SEAs works, by increasing n_{se} , η reduces due to smaller temperature difference of the fluids, and P increases due to more operating engines. For Type 4, by checking results, it can be found that when $n_{se} = 13$, the last engine doesn't work; when $n_{se} = 14$, only the first 10 engines will work; when $n_{se} = 15$, the working engine number drops to 9. For Type 5, by checking results, it can be found that when $n_{se} = 12$, the last 2 engines stop working; when $n_{se} = 13$, only the first 8 engines will work; when $n_{se} = 14$, the working engine number drops to 6; when $n_{se} = 15$, the working engine number drops to 4.

For a certain connection type, increase n_{se} will reduce the efficiency of SEA. For some connection types, increase n_{se} will reduce the output power P due to inoperative engines and smaller output power engines. Thus it is important to choose the number of engines for some connection types of SEA.

6. Conclusion

A new way to overcome the limitation of small engine capacity in dish-Stirling system by using SEA was proposed in this paper. Connection type may change the flow rates and temperatures of the fluids, as a result the performance of the SEA will be different depending on

the connection schemes. In order to compare performance of SEAs with different connections, five basic connection types of SEA were summed up according to flow type and flow order.

Analytical Stirling engine model was created to develop the SEA models for the investigation of influence of connection types. Imperfect regeneration and cycle irreversibility of Stirling engine cycle and heat exchange process between fluids and engine were considered in the model. Algorithm to numerically solve different connection types of SEA was developed. The model was evaluated by considering the prototype GPU-3 Stirling engine as a case study. Result shows that the proposed model predicted the performance with higher accuracy than Simple model [32] and Simple II model [35].

Models of SEAs were developed to calculate the performance under different parameters to find out the impacts of $T_{i,h}$, $q_{m,h}c_{p,h}$, $q_{m,c}c_{p,c}$ and n_{se} on different connection types. It was found that, as expected, decrease $T_{i,h}$ and $q_m c_p$ will weaken the performance of SEA of all connection types. However, for some connection types, there exists a critical temperature below which some engines stop working. This needs to be considered for SEA connection type selection, especially when $T_{i,h}$ is low. For given heating and cooling fluids, Type 2 has the best performance and adaptability. Type 2 and Type 3 have similar performance under different parameters ($T_{i,h}$, $T_{i,c}$ and $q_m c_p$), which means the flow order has little influence on the performance of an SEA. SEA of serial flows has the best performance and adaptability under different parameters. Given heating and cooling fluids, using serial flow is the best choice for the connection type of an SEA.

It is important to note that, in the future researches, the experiments of influence of connection type on SEA's performance can be carried out to verify the conclusions in this paper.

Acknowledgement

We gratefully acknowledge the support of International S&T Cooperation Program of China, under Grant No. 2014DFA60990, without which the present study could not have been completed.

Nomenclature

| | | | |
|----------|---|-------------------|---|
| A | heat transfer area (m^2) | γ_L | space ratio in process 34 |
| c_p | specific heat at constant pressure ($\text{J}\cdot\text{kg}^{-1}\cdot\text{K}^{-1}$) | μ | dynamic viscosity ($\text{kg}\cdot\text{m}^{-1}\cdot\text{s}^{-1}$) |
| c_v | specific heat at constant volume ($\text{J}\cdot\text{kg}^{-1}\cdot\text{K}^{-1}$) | Subscripts | |
| e | regenerator effectiveness | c | cooling fluid |
| J | annular gap cylinder displacer (m) | cw | cooler wall |
| K | dead volume factor | h | heating fluid |
| k | specific heat ratio (c_p/c_v), thermal conductivity ($\text{W}\cdot\text{m}^{-1}\cdot\text{K}^{-1}$) | hw | heater wall |
| m | mass of working fluid in Stirling engine (kg) | i | inlet |
| n_{se} | number of Stirling engine in SEA | o | outlet |
| P | power of Stirling engine (W) | p | piston |
| p | pressure (Pa) | r | regenerator |
| Q | absorbed heat (J) | th | theoretical |
| q_m | mass flow rate ($\text{kg}\cdot\text{s}^{-1}$) | | |
| R | gas constant ($\text{J}\cdot\text{kg}^{-1}\cdot\text{K}^{-1}$) | | |
| s_{se} | speed of Stirling engine (Hz) | | |
| T_H | working fluid temperature in the hot space (K) | | |
| T_L | working fluid temperature in the cold space (K) | | |
| T_R | effective working fluid temperature in regenerator (K) | | |
| T_w | wall temperature (K) | | |
| U | overall heat transfer coefficient ($\text{W}\cdot\text{m}^{-2}\cdot\text{K}^{-1}$) | | |
| V_C | compression volume (m^3) | | |
| V_D | total dead volume (m^3) | | |
| V_E | expansion volume (m^3) | | |
| V_{DC} | cold space dead volume (m^3) | | |
| V_{DH} | hot space dead volume (m^3) | | |
| V_{DR} | regenerator dead volume (m^3) | | |
| W | output work (J) | | |
| Z | displacer stroke (m) | | |

Abbreviations

SEA Stirling engine array

625 Greek Symbols

γ_H space ratio in process 12

- [1] Cheng, Z., He, Y., Cui, F.. A new modelling method and unified code with mcrt for concentrating solar collectors and its applications. *Applied Energy* 2013;101:686 – 698.
- [2] Qianjun, M., Ming, X., Yong, S., Yuan, Y.. Study on solar photo-thermal conversion efficiency of a solar parabolic dish system. *Environmental Progress & Sustainable Energy* 2014;33(4):1438–1444.
- [3] Wang, M., Siddiqui, K.. The impact of geometrical parameters on the thermal performance of a solar receiver of dish-type concentrated solar energy system. *Renewable Energy* 2010;35(11):2501 – 2513.
- [4] Wang, F., Shuai, Y., Tan, H., Zhang, X., Mao, Q.. Heat transfer analyses of porous media receiver with multi-dish collector by coupling mcrt and fvm method. *Solar Energy* 2013;93:158 – 168.
- [5] Zhu, J., Wang, K., Wu, H., Wang, D., Du, J., Olabi, A.. Experimental investigation on the energy and exergy performance of a coiled tube solar receiver. *Applied Energy* 2015;156:519 – 527.
- [6] Li, S., Xu, G., Luo, X., Quan, Y., Ge, Y.. Optical performance of a solar dish concentrator/receiver system: Influence of geometrical and surface properties of cavity receiver. *Energy* 2016;113:95 – 107.
- [7] Daabo, A.M., Mahmoud, S., Al-Dadah, R.K.. The effect of receiver geometry on the optical performance of a small-scale solar cavity receiver for parabolic dish applications. *Energy* 2016;114:513 – 525.
- [8] Loni, R., Kasaeian, A., Asli-Ardeh, E.A., Ghobadian, B., Roux, W.L.. Performance study of a solar-assisted organic rankine cycle using a dish-mounted rectangular-cavity tubular solar receiver. *Applied Thermal Engineering* 2016;108:1298 – 1309.
- [9] Wang, W., Xu, H., Laumert, B., Strand, T.. An inverse design method for a cavity receiver used in solar dish brayton system. *Solar Energy* 2014;110:745 – 755.
- [10] Craig, K.J., Marsberg, J., Meyer, J.P.. Combining ray tracing and cfd in the thermal analysis of a parabolic dish tubular cavity receiver. *AIP Conference Proceedings* 2016;1734(1):030009.
- [11] Aichmayer, L., Spelling, J., Laumert, B.. Preliminary design and analysis of a novel solar receiver for a micro gas-turbine based solar dish system. *Solar Energy* 2015;114:378 – 396.
- [12] Lovegrove, K., Luzzi, A., Soldiani, I., Kreetz, H.. Developing ammonia based thermochemical energy storage for dish power plants. *Solar Energy* 2004;76(1–3):331 – 337.
- [13] Senft, J.R.. Theoretical limits on the performance of stirling engines. *International Journal of Energy Research* 1998;22(11):991–1000.
- [14] Costea, M., Petrescu, S., Harman, C.. The effect of irreversibilities on solar stirling engine cycle performance. *Energy Conversion and Management* 1999;40(15–16):1723 – 1731.
- [15] Prieto, J.I., Stefanovskiy, A.B.. Dimensional analysis of leakage and mechanical power losses of kinematic stirling engines. *Proceedings of the Institution of Mechanical Engineers, Part C: Journal of Mechanical Engineering Science* 2003;217(8):917–934.
- [16] Organ, A.J.. *Stirling Cycle Engines : Inner Workings and Design (1)*. Somerset, GB: Wiley; 2013. ISBN 9781118818404.
- [17] Kongtragool, B., Wongwises, S.. Investigation on power output of the gamma-configuration low temperature differential stirling engines. *Renewable Energy* 2005;30(3):465 – 476.
- [18] Thombare, D., Verma, S.. Technological development in the stirling cycle engines. *Renewable and Sustainable Energy Reviews* 2008;12(1):1 – 38.
- [19] Lombardi, K., Ugursal, V., Beausoleil-Morrison, I.. Proposed improvements to a model for characterizing the electrical and thermal energy performance of stirling engine micro-cogeneration devices based upon experimental observations. *Applied Energy* 2010;87(10):3271 – 3282.
- [20] Ohtomo, M., Isshiki, N.. Basic performance of a three-temperature stirling cycle machine using vector analysis. *Nihon Kikai Gakkai Ronbunshu B Hen/transactions of the Japan Society of Mechanical Engineers Part B* 1995;61(591):4219–4225.
- [21] Wang, J.T., Chen, J.. Influence of several irreversible losses on the performance of a ferroelectric stirling refrigeration-cycle. *Applied Energy* 2002;72(2):495 – 511.
- [22] Rogdakis, E., Bormpilas, N., Koniakos, I.. A thermodynamic study for the optimization of stable operation of free piston stirling engines. *Energy Conversion and Management* 2004;45(4):575 – 593.
- [23] Kongtragool, B., Wongwises, S.. Thermodynamic analysis of a stirling engine including dead volumes of hot space, cold space and regenerator. *Renewable Energy* 2006;31(3):345 – 359.
- [24] Puech, P., Tishkova, V.. Thermodynamic analysis of a stirling engine including regenerator dead volume. *Renewable Energy* 2011;36(2):872 – 878.
- [25] Formosa, F., Despesse, G.. Analytical model for Stirling cycle machine design. *Energy Conversion and Management* 2010;51(10):1855–1863.
- [26] Shaizy, J., Hafez, A., Shenawy, E.E., Eteiba, M.. Simulation, design and thermal analysis of a solar stirling engine using matlab. *Energy Conversion and Management* 2014;79:626 – 639.
- [27] Cullen, B., McGovern, J.. Development of a theoretical decoupled stirling cycle engine. *Simulation Modelling Practice and Theory* 2011;19(4):1227 – 1234.
- [28] Cheng, C.H., Yang, H.S.. Optimization of geometrical parameters for stirling engines based on theoretical analysis. *Applied Energy* 2012;92:395 – 405.
- [29] Ahmadi, M.H., Sayyaadi, H., Dehghani, S., Hosseinzade, H.. Designing a solar powered stirling heat engine based on multiple criteria: Maximized thermal efficiency and power. *Energy Conversion and Management* 2013;75:282 – 291.
- [30] Ahmadi, M.H., Sayyaadi, H., Mohammadi, A.H., Barranco-Jimenez, M.A.. Thermo-economic multi-objective optimization of solar dish-stirling engine by implementing evolutionary algorithm. *Energy Conversion and Management* 2013;73:370 – 380.
- [31] Tursunbaev, I.A.. Analytic model of solar power plant with a stirling engine. *Applied Solar Energy* 2007;43(1):13–16.
- [32] Urieli, I., Berchowitz, D.M.. *Stirling cycle engine analysis*. Bristol: A. Hilger; 1984.
- [33] Ni, M., Shi, B., Xiao, G., Peng, H., Sultan, U., Wang, S., et al. Improved simple analytical model and experimental study of a 100 w beta-type stirling engine. *Applied Energy* 2016;169:768 – 787.
- [34] Jia, B., Smallbone, A., Feng, H., Tian, G., Zuo, Z., Roskilly, A.. A fast response free-piston engine generator numerical model for control applications. *Applied Energy* 2016;162:321 – 329.
- [35] Strauss, J.M., Dobson, R.T.. Evaluation of a second order simulation for sterling engine design and optimisation. *Journal of Energy in Southern Africa* 2010;21(2):17–29.
- [36] Abbas, M.. Thermal analysis of stirling engine solar driven. *Cder Dz* 2014;70(3):503–514.
- [37] Araoz, J.A., Salomon, M., Alejo, L., Fransson, T.H.. Numerical simulation for the design analysis of kinematic stirling engines. *Applied Energy* 2015;159:633 – 650.
- [38] Babaelahi, M., Sayyaadi, H.. A new thermal model based on polytropic numerical simulation of stirling engines. *Applied Energy* 2015;141:143 – 159.
- [39] Barreto, G., Canhoto, P.. Modelling of a stirling engine with parabolic dish for thermal to electric conversion of solar energy. *Energy Conversion and Management* 2017;132:119 – 135.
- [40] Wu, F., Chen, L., Wu, C., Sun, F.. Optimum performance of irreversible stirling engine with imperfect regeneration. *Energy Conversion and Management* 1998;39(8):727 – 732.
- [41] Yaqi, L., Yaling, H., Weiwei, W.. Optimization of solar-powered stirling heat engine with finite-time thermodynamics. *Renewable Energy* 2011;36(1):421 – 427.
- [42] Hosseinzade, H., Sayyaadi, H., Babaelahi, M.. A new closed-form analytical thermal model for simulating stirling engines based on polytropic-finite speed thermodynamics. *Energy Conversion and Management* 2015;90:395 – 408.
- [43] Ahmadi, M.H., Ahmadi, M.A., Pourfayaz, F., Bidi, M., Hos-

- seinzade, H., Feidt, M.. Optimization of powered stirling heat engine with finite speed thermodynamics. *Energy Conversion and Management* 2016;108:96 – 105.
- [44] Chen, L., Zhang, W., Sun, F.. Power, efficiency, entropy-generation rate and ecological optimization for a class of generalized irreversible universal heat-engine cycles. *Applied Energy* 2007;84(5):512 – 525.
- [45] Ahmadi, M.H., Ahmadi, M.A., Mellit, A., Pourfayaz, F., Feidt, M.. Thermodynamic analysis and multi objective optimization of performance of solar dish stirling engine by the centrality of entransy and entropy generation. *International Journal of Electrical Power & Energy Systems* 2016;78:88 – 95.
- [46] Li, R., Grosu, L., Queiros-Conde, D.. Multi-objective optimization of stirling engine using finite physical dimensions thermodynamics (fpdt) method. *Energy Conversion and Management* 2016;124:517 – 527.
- [47] Patel, V., Savsani, V.. Multi-objective optimization of a stirling heat engine using ts-tlbo (tutorial training and self learning inspired teaching-learning based optimization) algorithm. *Energy* 2016;95:528 – 541.
- [48] Luo, Z., Sultan, U., Ni, M., Peng, H., Shi, B., Xiao, G.. Multi-objective optimization for gpu3 stirling engine by combining multi-objective algorithms. *Renewable Energy* 2016;94:114 – 125.
- [49] Organ, A.J.. The regenerator and the stirling engine. Mechanical Engineering Publications Limited 1997;.
- [50] Duan, C., Wang, X., Shu, S., Jing, C., Chang, H.. Thermodynamic design of stirling engine using multi-objective particle swarm optimization algorithm. *Energy Conversion & Management* 2014;84:88–96.
- [51] Heywood, , JohnB, . Internal combustion engine fundamentals. McGraw-Hill; 1988.
- [52] Timoumi, Y., Tlili, I., Nasrallah, S.B.. Design and performance optimization of gpu-3 stirling engines. *Energy* 2008;33(7):1100 – 1114.
- [53] MARTINI, W.R.. Stirling engine design manual, 2nd edition. Tech. Rep.; Martini Engineering, Richland, WA (USA); 1983.
- [54] Hooshang, M., Moghadam, R.A., AlizadehNia, S.. Dynamic response simulation and experiment for gamma-type stirling engine. *Renewable Energy* 2016;86:192 – 205.